JOURNAL OF STRUCTURAL BIOLOGY **118,** 140–148 (1997)
ARTICLE NO. SB973840

Three-Dimensional Cryoelectron Microscopy of 16-Protofilament Microtubules: Structure, Polarity, and Interaction with Motor Proteins

K. Hirose[1] and W. B. Amos

MRC Laboratory of Molecular Biology, Hills Road, Cambridge, CB2 2QH United Kingdom

A. Lockhart and R. A. Cross

Marie Curie Institute, The Chart, Oxted, Surrey, RH8 0TL, United Kingdom

and L. A. Amos

MRC Laboratory of Molecular Biology, Hills Road, Cambridge, CB2 2QH United Kingdom

Received September 8, 1996, and in revised form December 18, 1996

We present a three-dimensional (3D) map, reconstructed from electron microscope (EM) images of naturally occurring 16-protofilament (PF) microtubules (MTs) in ice. We compare it with the tubulin in six 3D maps of MTs decorated with motor domains, three from frozen MTs decorated with kinesin or ncd in the tightly bound AMP–PNP state, and three from negatively stained MTs decorated with kinesin in different nucleotide states. The comparison confirms that kinesin and ncd bind to identical sites and interact with both monomers of a tubulin dimer. Maps of specimens in negative stain and in ice are similar except that the protein in the top half of a motor domain appears denser in negative stain. The interactions have only a small effect on tubulin structure; the outward appearance is unchanged, but there seems to be a small internal rearrangement. The relative polarity of undecorated and decorated MTs is evident from their 3D structures. This agrees with the absolute polarities indicated by the orientations of motors in decorated specimens and by polar superposition patterns calculated for undecorated MTs. An image of tubulin PFs in zinc-induced sheets has been tentatively oriented by similar criteria.

INTRODUCTION

One of the important functions of microtubules (MTs)[2] is to direct intracellular transport with the aid of motor molecules (Thaler and Haimo, 1996; Kellogg *et al.*, 1994). Structural aspects of MT polarity and the interactions between MTs and motor molecules are, therefore, of great interest (Mandelkow and Mandelkow, 1995; Amos and Hirose, 1997; Amos and Cross, 1997). Song and Mandelkow (1995) first showed that saturating levels of the head domains of kinesin bound to sheets of tubulin protofilaments (PFs) produced a characteristic polar pattern of high, low, and intermediate densities, when viewed by negative stain electron microscopy (EM). They and others, including ourselves (Hirose *et al.*, 1995a,b; Hoenger *et al.*, 1995; Kikkawa *et al.*, 1995), attempted to relate this polarity to the minus (assembly-initiating) and plus (growing) ends of natural MTs, by decorating MTs and sheets grown from the ends of flagellar axonemes. Since the technique is subject to artifacts unless carried out very carefully, different groups obtained different answers (detailed in Amos and Hirose, 1997). This confusion affected the significance of our finding that a part of the kinesin motor domain undergoes a tilting movement when ADP is lost from its binding site (Hirose *et al.*, 1995b). According to our determination of MT polarity, the tilting was toward the plus end and could, therefore, be important in the plus-wards movement of kinesin. In this paper, we confirm that all current markers of microtubule polarity are consistent and agree with our original conclusions.

To understand the movement of motors along MTs, it is also important to establish the extent to which changes in the MT itself may contribute to the motion. The conformations of tubulin sheets and 10-PF MTs decorated with kinesin or ncd in a strongly attached state have been compared by Kikkawa *et al.* (1995) and by Hoenger *et al.* (1995)

[1] Present address: International Institute for Advanced Research, Matsushita Electric Industrial Co. Ltd., 3-4 Hikaridai, Seika, Kyoto 619-02, Japan.

[2] Abbreviations used: MT, microtubule; PF, protofilament; ncd, nonclaret disjunctional protein.

1047-8477/97 $25.00

with undecorated structures and significant changes were reported by Hoenger *et al.* (1995). It is possible that some part of the apparent change in the latter work was due to the use of tubulin sheets; because EM specimens cannot be tilted in all directions, the data lack information about how the density varies with depth through the specimen. In this paper, we compare the three-dimensional (3D) structures of 16-PF MTs with and without attached motors; these specimens provide a full range of views in a single image. We conclude that the attachment of motors has no detectable effect on the tubulin lattice and that changes in the internal conformations of tubulin molecules are small and subtle.

MATERIALS AND METHODS

Electron Microscopy

Testes were dissected from male crickets (*Acheta domesticus*) and homogenized in a small hand homogenizer in extracting solution (5 m*M* Pipes, 0.5 m*M* EGTA, 2 m*M* $MgSO_4$, 1 m*M* DTT, 10 μ*M* taxol, pH 7.0). Solutions of partially purified axonemes were obtained by spinning down sperm heads and other contaminants, as already described (Hirose *et al.*, 1995b, 1996). The solution was applied as a thin layer to EM grids covered with a holey carbon film and rapidly frozen by plunging the grids into an ethane slush. The ice-embedded specimens were examined using a Gatan cold stage in a Philips EM 420 microscope, operating at 120 kV. Images were recorded at a magnification of 36 000 and a defocus of 1300–1600 nm.

Cryo-EM images reported elsewhere (Hirose *et al.*, 1996) are of MTs decorated with single- or double-headed kinesin motor domains (expressed from rat kinesin heavy chain constructs) or with double-headed *Drosophila* ncd (nonclaret disjunctional) protein (Lockhart *et al.*, 1995), in solutions including 0.5–2.0 m*M* AMP–PNP. Negatively stained specimens consisted of MTs decorated with single-headed kinesin in solutions containing AMP–PNP, ADP, or apyrase (to deplete residual ATP or ADP) (Hirose *et al.*, 1995b). These samples were applied to plain carbon grids before staining with uranyl acetate and were imaged at a magnification of 45 000.

Image Analysis

Micrographs were densitometered in 20-μm steps and the digitized images processed as before (Hirose *et al.*, 1995b, 1996). After correction for any curvature, 569-nm stretches of MT were boxed off for the calculation of 512 × 1024 Fourier transforms. Because different helical families on each nominal layer line (equatorial, 8 and 4 nm (see Fig. 1)) do not overlap but actually lie on separate lines, one image of a 16-PF MT can provide two sets of data for the calculation of 3D density maps. The maps were averaged in real space, after being scaled so that the mean density was 0 and their power (*P*, the sum of densities squared) was 1 (Trachtenberg *et al.*, 1987). The values of *P* for various averages provided further criteria for choosing the most consistent data sets.

RESULTS

Electron Microscopy of Cricket MTs

When cricket testes were dispersed in a low ionic strength medium, the membrane around the sperm tails lysed to expose the axonemes. Each axoneme consists of a cylinder of nine doublet MTs and associated 16-PF singlet accessory microtubules, enclosing a pair of singlet 13-PF MTs (Dallai and Afzelius, 1990). Where the ends of the axonemes were frayed, it was possible to obtain EM images of individual MTs (Hirose *et al.*, 1995b, 1996).

The central-pair MTs are easily identified by their smaller diameters (not shown) but, from some angles, outer doublets appear similar to 16-PF singlets (Figs. 1a–1d). However, their optical or computed diffraction patterns have different features. The patterns from doublet MTs (Figs. 1b′ and 1d′) include straight rows of reflections at ¼ and ⅛ nm^{-1}; both layer lines are seen whether or not the specimens are decorated with motor domains. Peaks on the equator, at ~⅕ nm from the origin (marked by arrow), vary in strength depending on the rotation angle about the MT axis. The 16-PF MTs produce split layer lines (Figs. 1a′ and 1c′) with reflections at slightly different axial levels, always including off-equatorial pairs of reflections (arrow). For undeco-

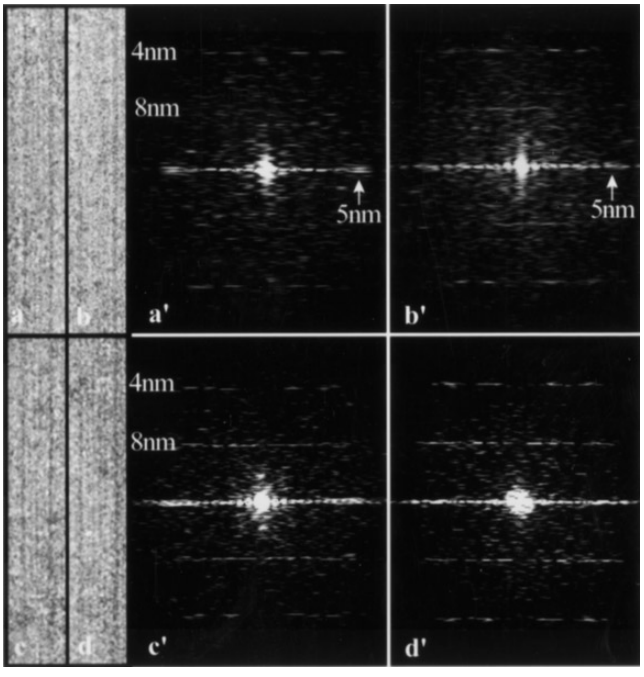

FIG. 1. EM images of insect axonemal MTs in ice (a–d) and their computed diffraction patterns (a′–d′). (a and c) 16-PF singlet accessory MTs; (b and d) doublet MTs. (a and b) undecorated; (c and d) decorated with saturating levels of bacterially expressed kinesin motor domains. Because 16-PF MTs are slightly twisted, their diffraction patterns (a′ and c′) have intensity peaks just above and below the equatorial line; different contributions to the 4-nm layer lines are at slightly different heights above the equator; in diffraction patterns (b′ and d′) from doublet MTs, which have no twist, the pairs of equatorial reflections merge and often interfere destructively. The 8-nm layer line of 16-PF MTs is greatly enhanced by decoration (c′); natural accessory proteins contribute to the 8-nm layer line of doublets (b′) but addition of kinesin increases its intensity (d′).

rated 16-PF specimens, imaged in either ice or uranyl acetate, the 8-nm layer line is often barely detectable (Fig. 1a′).

Comparison of Undecorated and Decorated MTs

Figure 2a shows a surface map of the undecorated 16-PF MT, calculated by averaging six data sets. The outside surfaces of 16-PF MTs decorated with various motor domain constructs have been described (Hirose *et al.*, 1995b, 1996). Parts of three structures imaged in ice are shown in Figs. 2c–2e and compared with the undecorated MT (Fig. 2b). The inside surfaces of undecorated and decorated MTs are very similar and the only obvious differences on the outside surfaces are the attached motors. Diffraction patterns show no detectable change in the MT lattice spacing. Any conformational changes in tubulin due to interaction with kinesin and ncd must, therefore, be localized and have no effect on the dimensions of the subunits or the bonds with neighboring subunits.

We looked for localized changes in sections through the MTs. There are none apparent in transverse

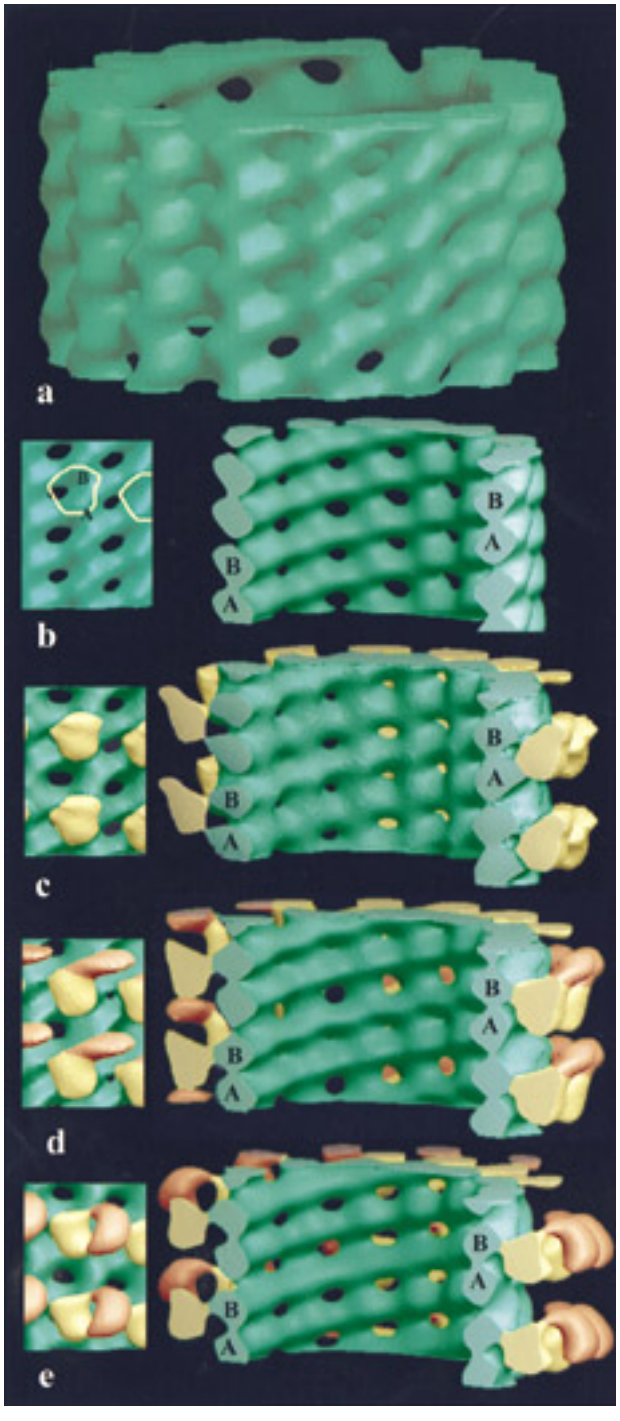

FIG. 2. 3D models computed from digitized images of 16-PF MTs. The surfaces shown represent one contour level in each 3D density map (calculated as in Vigers *et al.*, 1986). (a) A 16-nm-high segment of undecorated MT from an average of three cryo-EM images such as Fig. 1a. The 4-nm tubulin monomer periodicity along each PF is clear but in this view there is no apparent 8-nm periodicity. (b–e) Comparison of regions of the outside (left) and inside surfaces (right) of undecorated (b) and decorated (c–e) MTs imaged in ice (Hirose *et al.*, 1996). Tubulin heterodimers are not obvious on inside or outside surfaces but the pairing of tubulin monomers (labeled A and B) is detectable where PFs have been cut. The strong longitudinal (inter-PF) grooving on the outside and continuous transverse ridges on the inside surfaces agree well with earlier images of MTs (e.g., Amos and Klug, 1974). The outside surfaces of (c–e) are decorated, with single-headed kinesin in c, double-headed kinesin in d, and double-headed ncd in e. All the decoration was in the presence of AMP–PNP. Bound heads are colored yellow, second heads, not bound directly to tubulin, are colored orange. The site on tubulin to which the first heads bind is outlined in b.

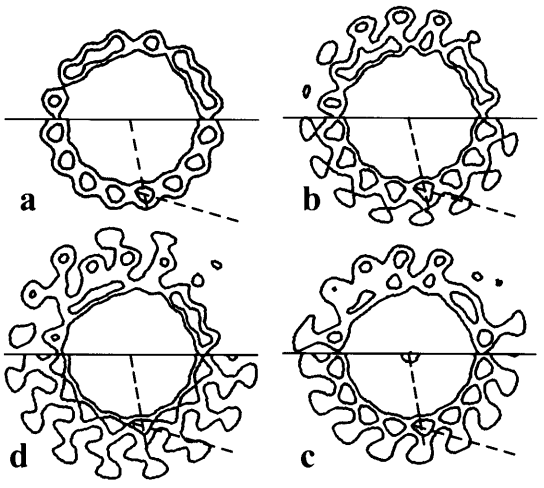

FIG. 3. Contoured cross sections through 3D maps (upper half of each panel) of 16-PF MTs in ice, undecorated (a) or decorated (b with single kinesin heads, c with double kinesin heads, d with double-headed ncd). The lower halves show average densities projected along the PF axes. In each case, the long axis of a projected PF and a radial line are shown (dashed), to illustrate the anticlockwise slewing.

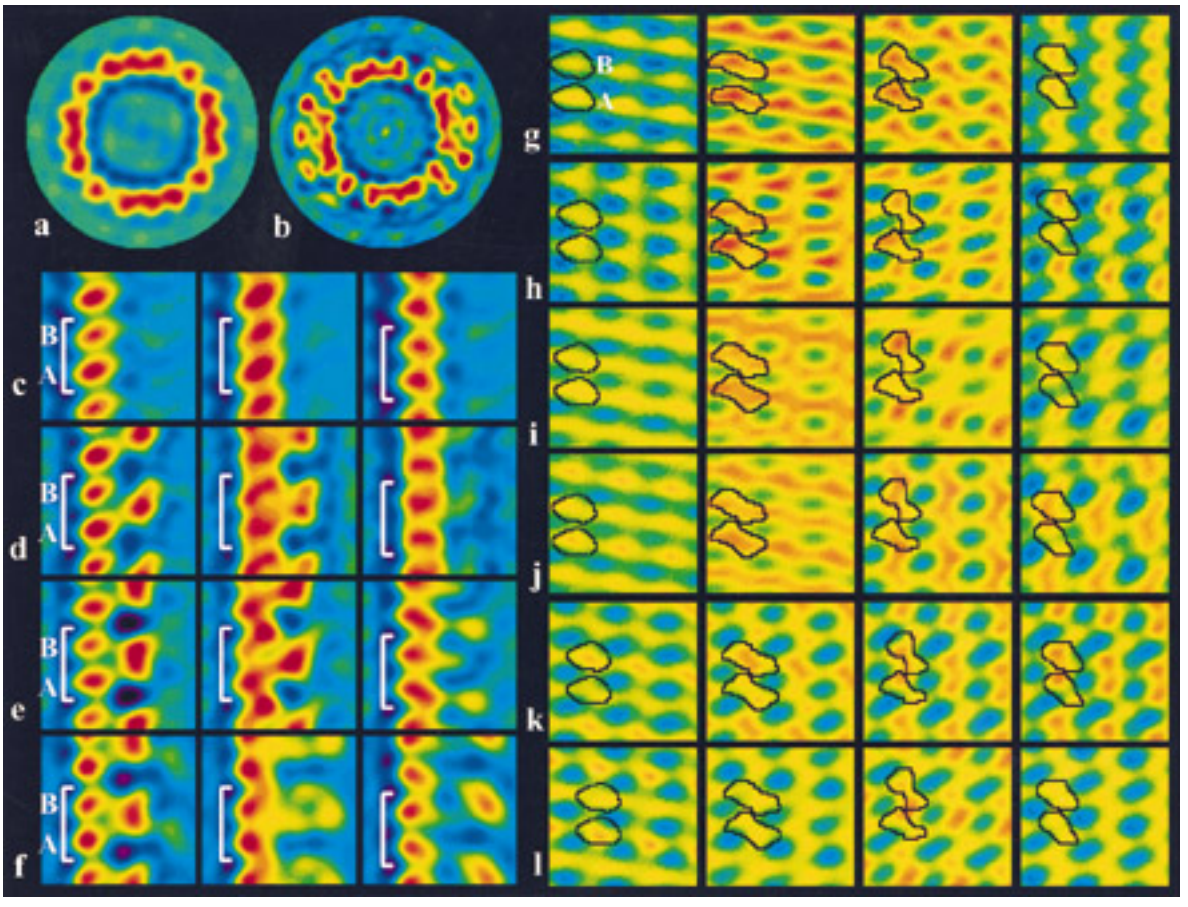

FIG. 4. Sections through 3D density maps with the density levels graded by color (red, high protein density; blue, stain or ice). (a and b) The cross sections in Figs. 3a and 3b in more detail. (c–f) Each show three axial sections through the cryo-EM structures: c is the undecorated MT (average of six sets of data); d is a MT decorated with single-headed kinesin (average of four); e is a MT decorated with double-headed kinesin (average of two); f is a MT decorated with double-headed ncd (average of five). Brackets enclose tubulin dimers; labeling of A and B as in Fig. 2. (g–l) Cylindrical sections through 3D maps of undecorated (g) and decorated MTs (h–l), at 4 radii (12.3, 13.5, 14.7, and 15.9 nm) within the MT density. Putative tubulin dimer units are outlined in each section; the same outline has been superimposed on all decorated structures, to aid comparison. (g–j) Images from structures in ice (Figs. 1 and 2) (h–j, decorated with single-headed kinesin, double-headed kinesin, and double-headed ncd, all with AMP–PNP). (k–l) Images from MTs decorated with single-headed kinesin, under different nucleotide conditions (with AMP–PNP or ADP), and imaged in negative stain.

sections (Figs. 3, 4a and 4b) but longitudinal sections through the PFs show small changes. Two tubulin monomers (labeled A and B) show very similar shapes and orientations in the sections of undecorated MTs (Fig. 4c), whereas A and B subunits in decorated MTs (Figs. 4d–4f) are clearly different, especially in the second and third columns. Compared with Fig. 4c, subunit B in the third column of Figs. 4d–4f appears to make closer contact with the monomer above it, near the outside surface. This feature is the same whether the bound motor is kinesin or ncd.

The structures can be compared in more detail in cylindrical sections (Figs. 4g–4j. At lower radii, no significant differences are seen, but there appears to be a change by the third column. Compared with Fig. 4g, the subunit A in Figs. 4h–4j appears to have rotated about 10° clockwise, as viewed from outside the MT.

Comparison of Complexes in Ice and in Negative Stain

The relative contrast of structures imaged in ice and in negative stain is reversed because protein is denser than ice but much less dense than heavy metal stain. Allowing for this, the results obtained by the two techniques are quite similar (Hirose *et al.*, 1995b, 1996), as shown here in cylindrical sections (Figs. 4h–4l) and projected axial cross sections (Figs. 5a–5d). Cross sections best show the polarity of a MT decorated with single heads; lines from the MT center through tubulin to the attached head have a clockwise slew when the MT is viewed from the plus end, as described by Sosa and Milligan (1996).

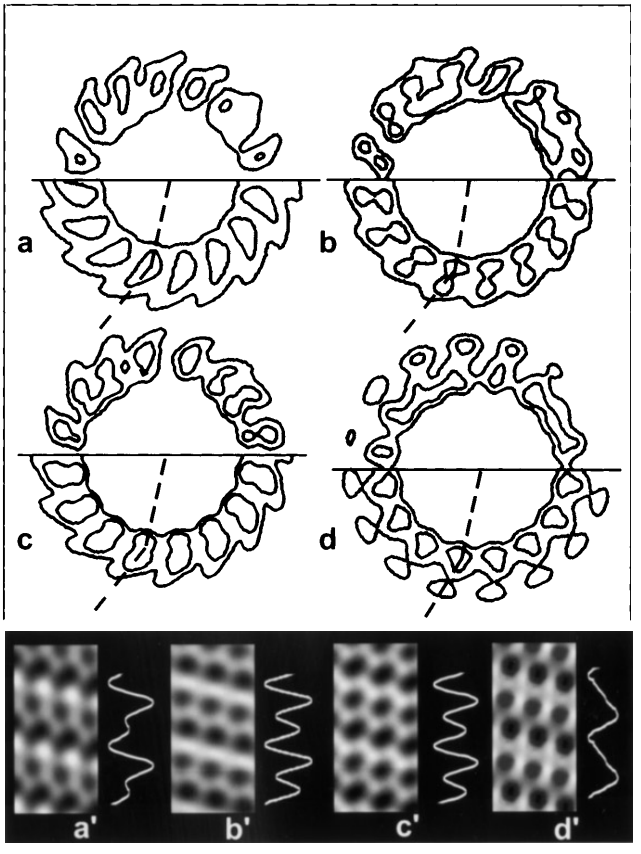

FIG. 5. Relative polarities of MTs decorated with single-headed kinesin: (a–d) contoured cross sections through 3D maps and projected densities, as in Fig. 3. Dashed lines indicate the clockwise slewing of the attached heads. (a′–d′) Cylindrical projections calculated by summing the densities in cylindrical sections over all radii, including sections through the kinesin heads; the result is roughly equivalent to the EM image of a decorated tubulin sheet. Alongside each image is a graph of the average density across a PF. (a–c and a′–c′). The three negatively stained single-headed structures (a with AMP–PNP, b with no nucleotide, c with ADP); (d and d′) the single-headed kinesin-decorated structure in ice (with AMP–PNP).

The sum of cylindrical sections at all radii of a MT map is roughly equivalent to an EM image of an opened-out tubulin sheet. Thus, 2D images calculated from the maps of decorated MTs in negative stain (Figs. 5a′–5c′) resemble images of negatively stained decorated sheets (Hirose *et al.*, 1995b). The sequence of peaks and troughs in plots of integrated density across a PF confirms that the negatively stained structures are oriented plus-end upward (cf. Hirose *et al.*, 1995a). On the other hand, the density plot obtained from a decorated MT in ice (Fig. 5d′) looks quite different, even though the 2D image itself is basically similar to the negatively stained images.

Polarity of Undecorated PFs

Polarities of the 3D maps of undecorated MTs were first determined by comparing them with the decorated MTs. In the projected cross sections (lower halves of Figs. 3a–3d), the long axis of a projected PF slews anticlockwise in all cases, in agreement with Sosa and Milligan (1996). Similarities in the tubulin structures of undecorated and decorated MTs as seen in the surface maps (Fig. 2), longitudinal sections (Figs. 4c–4f), and cylindrical sections (Figs. 4g–4l) confirm this relative polarity.

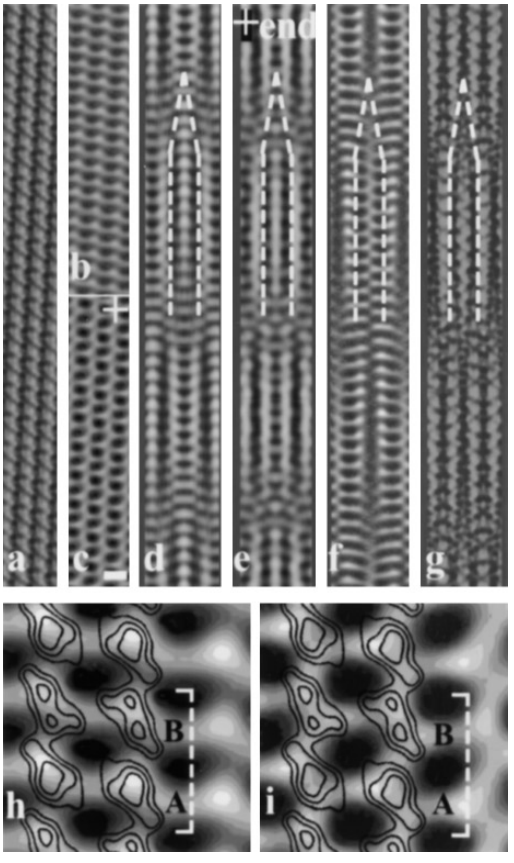

FIG. 6. Projected images of tubulin. (a) Projected images of PFs from zinc–tubulin sheets (Baker and Amos, 1978), rearranged into the normal lattice. (b and c) Cylindrical projections calculated by summing the densities only within the MT: b is from the undecorated MT (Figs. 2a, 2b, 3a); c is from a decorated MT of known polarity (Figs. 2c, 3b, 4d). (d and e) Images that show b and c superimposed on their mirror images, mirrored about the long axes to simulate the central features of "4-start" MTs with right-handed PFs, as in our original 16-PF MTs. Polar features of the patterns, such as those inside the boxes, indicate that their relative polarities are the same. (f and g) The effects of superimposing b and a on their mirror images with an axial shift of 6 nm, mimicking the projected images of "3-start" MTs with right-handed PFs. On the axis of each image there are upwardly pointing white (inside dashed box) and black spikes (below dashed box). (h and i) Enlarged views of b and c; differences between α- and β-tubulin are only obvious in i. Contours representing zinc–tubulin PFs have been superimposed in two possible orientations, of which the second corresponds to a and to that of the 3D image published by Nogales *et al.* (1995); results obtained by these authors when labeling β-tubulin with taxol suggest that subunits A and B correspond, respectively, to α- and β-tubulin monomers.

Images of undecorated PF arrays, calculated either from undecorated MTs or from a subset of cylindrical sections through decorated MTs, show a weak polarity (Figs. 6b and 6c). Figures 6d and 6e show moiré patterns produced by rotating each image a few degrees, to simulate PFs with a helical twist, and then superimposing it on its mirror image. The result, which is roughly equivalent to a filtered image of the original MT, amplifies the polar features and confirms that the relative orientation of the two maps is correct. Shifting the mirror image axially by 6 nm, before superposing it on the original, simulates the pattern from a MT with a 3-start family of shallow helices (Fig. 6f).

Identification of Two Tubulin Monomers and Comparison with Zinc-Induced Sheets

The 8-nm periodicity due to differences between alternate tubulin monomers is weak in the diffraction patterns of undecorated MTs (Fig. 1a′). Differences between two monomers are not clear in the surface maps, but show up in sections (Figs. 4c–4l, also see the cut surfaces in Fig. 2). There are consistent differences between the monomers in the undecorated and decorated samples that allow us to tentatively label monomers A and B in different specimens. Figures 2 and 4d–4f show that kinesin and ncd bind to the MTs in the same manner, making contacts with both a B subunit and the A subunit below.

Images of undecorated tubulin were also compared in projection with PFs seen in zinc-induced tubulin sheets (Baker and Amos, 1978; Wolf *et al.*, 1993). In 3D images of these sheets (Amos and Baker, 1979; Nogales *et al.*, 1995), one of the exposed surfaces of individual PFs is more rugged and is assumed to correspond to the inside of a MT (see Fig. 2). The projected image in Fig. 6a is thus predicted to correspond to a view from the outside of a MT, but there are two possible orientations relative to our projected images of MTs (see contours in Figs. 6h and 6i). In both cases, the subunit identified as β-tubulin in the zinc-induced sheets has been superimposed on tubulin subunit B of the MT models (see Discussion). The orientation in Fig. 6a corresponds to the second in Figs. 6h and 6i and has been used to produce the moiré pattern in Fig. 6g. The polarity of this final moiré pattern is, however, not very clear.

DISCUSSION

Lanzavecchia *et al.* (1994) first reconstructed 3D images of 16-PF MTs from insects. Their specimens were negatively stained with sodium phosphotungstate and, in projection, showed dumbbell-shaped tubulin dimers similar to those seen in equivalently stained flagellar A tubules (Amos and Klug, 1974). Pairing of the tubulin monomers is less obvious in images of specimens stained with uranyl acetate (unpublished data) or of the unstained, frozen-hydrated microtubules studied here. But 3D images of all three types of specimen agree in that they show less difference between neighboring monomers on their surfaces than in their internal density distributions. This would suggest that phosphotungstate binds to tubulin and emphasizes an internal difference between α- and β-monomers.

Microtubule Polarity

The 3D images of undecorated MTs and those decorated with kinesin or ncd motor constructs all show a very similar structure for tubulin. Polar features are apparent in cylindrical sections (Figs. 4g–4i outer radii) and projections (Figs. 5a′–5d′), as well as the slight slewing of the PFs in views projected down the axis (Figs. 3, and 5a–5d). These observations allow us to orient all the 3D images relative to one another, unambiguously. In previous work (Hirose *et al.*, 1995a,b) we determined the orientation of decorated MT structures by comparison with the polar pattern visible on decorated tubulin sheets growing from the ends of flagellar axonemes. The issue was, however, confused by accompanying papers (see Hackney, 1995). Hoenger *et al.* (1995), who reported the opposite polarity for decorated axonemes, have recently reversed their conclusion after obtaining new results from MTs nucleated by centrosomes and whole sea urchin sperm (Hoenger and Milligan, 1996a). Mandelkow *et al.* (personal communication) have similarly retracted the original conclusion of Song and Mandelkow (1995).

Kikkawa *et al.* (1995) showed images of decorated tubulin sheets, associated with axonemes, which agreed with our findings but, when they compared these negatively stained images with a projected view of their 3D image, obtained from images of decorated 10-PF microtubules in ice, their interpretation was different from ours. In this paper, we have demonstrated that cylindrical projections of decorated MTs imaged in negative stain do indeed produce the same polar patterns as negatively stained sheets, in support of our original interpretation. However, a cylindrical projection from a 3D map of MTs imaged in ice does not produce the same pattern of peaks. It is not surprising, therefore, that Kikkawa *et al.* had difficulty orienting their 3D map relative to images of negatively stained sheets.

The density variation within the head domain is the one major difference between results obtained in ice and in negative stain. The MT structures themselves are roughly comparable at all radii, though

there are small shifts in the positions of the density peaks at inner radii (compare Figs. 4h–4j and 4k–4l). In both types of map, each bound motor molecule apparently makes more-or-less equal contacts with two adjacent monomers. But in negative stain the protein in the top half of the motor appears denser and produces a strong white stripe in projection (Figs. 5a′–5c′); possibly the structure there is particularly hydrophobic and stain-excluding. Thus, earlier work on negatively stained images (Song and Mandelkow, 1995; Hoenger *et al.*, 1995; Hirose *et al.*, 1995) emphasized the bond between the top part of the motor domain and one of the tubulin monomers.

Moiré Patterns

Chrétien *et al.* (1996) have investigated cryo-EM images of MTs grown from centrosomes in order to orient polar patterns first reported by Mandelkow *et al.* (1986). Although most MTs grown from centrosomes have 13 PFs, which do not rotate around the MT axis, a few consist of 12 PFs, which twist in a right-handed sense, or 14 PFs, which have a left-handed twist. Moiré patterns produced in the twisted MTs show an arrowhead motif, which apparently points toward the plus end if the PFs have a right-handed twist and toward the minus end if they are left-handed.

The 12- to 14-PF MTs have a lattice with a 3-start family of shallow helices (Wade and Chretién, 1993). The MTs in this study have a 4-start family of shallow helices and their 16-PFs have a right-handed twist. The superposition pattern produced by structures with 4-start helices is a less polar form of arrowhead; however, features of Figs. 6d and 6e obtained from 3D images of undecorated MTs and of decorated MTs with the motor density removed help to confirm that the relative orientation of the two maps is correct.

A MT with 3-start shallow helices and PFs with a right-handed twist is simulated in Fig. 6f, using data from the undecorated MT map. The arrowhead pattern pointing toward the plus end, in this case, provides further confirmation of the absolute polarity of our 3D structures, as Sosa and Milligan (1996) also found.

Identification of Tubulin Dimers

The relative polarities of tubulin PFs in MTs and in zinc-induced sheets is still uncertain. However, comparing the low-resolution shapes of the tubulin subunits (Fig. 6i) with the taxol-labeled tubulin of Nogales *et al.* (1995) suggests that monomer B is β-tubulin, while A is α-tubulin. Thus, of the two tubulin monomers making contact with an attached motor domain, the plus-wards monomer is probably β-tubulin. Images of the very ends of decorated tubulin sheets (Hirose *et al.*, 1995a) suggest that there are no extra unlabeled monomers there, which should mean that the pair of monomers associated with one motor domain (see Fig. 2) corresponds to a dimer subunit. The resulting conclusion, that β-tubulin occurs at the plus end, is supported by the results of Mitchison (1993), who used beads coupled to GTP to show that the exchangeable site for GTP is accessible only at the plus ends of microtubules, and of Fan *et al.* (1996), who labeled only the minus ends of microtubules with beads coated with an antibody to α-tubulin. Thus, three independent lines of evidence point to the conclusion that α-tubulin is at the minus end and β-tubulin at the plus end.

Interaction of Motor Molecules with Tubulin

It is clear from the maps in Figs. 2–4 that kinesin and ncd bind to essentially identical sites on tubulin, interacting with both monomers of a tubulin heterodimer. Chemical cross-linking studies have shown that kinesin can be cross-linked most easily to β-tubulin (Song and Mandelkow, 1994; Kikkawa *et al.*, 1994), but both motors can also be cross-linked to α-tubulin (Walker, 1995). Calculated difference maps (Hirose *et al.*, 1996) support the view that attached heads of kinesin and ncd are virtually indistinguishable. Both bind to the left side of the PF when the plus end of the MT is toward the top of the picture. In each case, it is possible that the motor also makes a weaker contact with the PF on its lefthand side. In neither case do the second heads of double-headed motors bind directly to tubulin, under these conditions (Figs. 2d–2e). Finally, we find that a small change to the internal structure of tubulin due to motor attachment is the same whichever motor is bound.

The structure of tubulin is being studied at higher resolution in the form of zinc-induced tubulin sheets (Nogales *et al.*, 1995). However, to use this information to better understand the interaction between tubulin and motors in our maps, it is necessary to know the plus–minus orientation of the zinc–tubulin PFs. In one of the two likely orientations (on the right in Figs. 6h and 6i), the strong kinesin/ncd binding site would be close to the taxol binding site and also to long α-helices believed to be part of the tubulin C-terminal domains (Nogales *et al.*, 1995). This orientation would provide the simplest explanation for competition experiments involving MTs, motor domains, and a peptide derived from the C-terminus of β-tubulin (Goldstein, 1995). The alternative would place the C-terminal domains of tubulin on the right side of the PF, distant from the strong motor binding site but near to a motor attached to the neighboring PF. In this case, the possible interaction of each motor with a second PF might be significant. The resolution of the normal tubulin

images in Figs. 6h and 6i is lower than the zinc–tubulin image and produces a less polar subunit shape. It is also likely, even if the PFs in the two types of polymer have very similar structures, that there is a small axial rotation between the views projected in each case. Thus, it is not possible to determine the relative orientation of the two images reliably. However, the peak densities overlap best in the case of the righthand alternative and the moiré patterns in Figs. 6f and 6g are marginally more similar in this relative orientation. Higher resolution images of undecorated normal tubulin sheets of known polarity (Hoenger and Milligan, 1995, 1996a,b) also resemble the zinc–tubulin PF images better in this orientation.

Changes in Tubulin Structure

It is difficult to be sure whether small changes in tubulin density are reliable when the presence of motors obviously produces a large change nearby. Hoenger *et al.* (1995, 1996b) have reported significant changes on the inside surface in images of decorated tubulin sheets, reconstructed from tilt series. Changes could appear artifactually on the inside surface because the resolution normal to a sheet is reduced by the inevitable difficulty in obtaining data in this direction. On the other hand, images of sheets tend to provide higher resolution in the first two dimensions than our isometric resolution. Therefore, the two types of analysis are complementary; images derived from tilted sheets may give a projected view of a change in more detail, whereas images from helically symmetrical specimens should be more reliable for locating the change. Our results suggest that most of the change is restricted to parts of the tubulin dimer in closest contact with a bound motor domain. Since some regions of tubulin are constant, it is likely that changes we see elsewhere are real. No changes are visible on either the inside surface of the MT or on regions of the outer surface not in direct contact with the motor, but subtle differences in the interior of the PFs may possibly be significant. However, the recent report (Turner *et al.*, 1996) that kinesin-coated beads move with the same velocity on glutaraldehyde-fixed microtubules as on taxol-stabilized microtubules would suggest that the main role of a microtubule in motility is to act as a stable substrate.

We thank Drs. Richard Henderson, Nigel Unwin, and Chikashi Toyoshima for help with cryoelectron microscopy techniques and Dr. Tony Crowther for reading the manuscript.

REFERENCES

Amos, L. A., and Baker, T. S. (1974) The three-dimensional structure of tubulin protofilaments, *Nature (London)* **279,** 607–612.

Amos, L. A., and Hirose, K. (1997) Microtubule-motor complexes, *Curr. Opin. Cell Biol.* **9**(1), 4–11.

Amos, L. A., and Cross, R. A. (1997) Structure and dynamics of molecular motors, *Curr. Opin. Struct. Biol.* **7**(2), in press.

Amos, L. A., and Klug, A. (1974) Arrangement of subunits in flagellar microtubules, *J. Cell Sci.* **14,** 523–549.

Baker, T. S., and Amos, L. A. (1978) Structure of the tubulin dimer in zinc-induced sheets, *J. Mol. Biol.* **123,** 89–106.

Chrétien, D., Kenney, J. M., Fuller, S. D., and Wade, R. H. (1996) Determination of microtubule polarity by cryo-electron microscopy, *Structure* **9,** 1031–1040.

Dallai, R., and Afzelius, B. A. (1990) Microtubular diversity in insect spermatozoa: Results obtained with a new fixative, *J. Struct. Biol.* **103,** 164–179.

Fan, J., Griffiths, A. D., Lockhart, A., Cross, R. A., and Amos, L. A. (1996) Microtubule minus ends can be labelled with a phage display antibody specific to alpha-tubulin, *J. Mol. Biol.* **259,** 325–330.

Goldstein, L. S. B. (1995) Structural features involved in force generation in the kinesin superfamily, *Biophys. J.* **68,** 260s–266s.

Hackney, D. D. (1995) Motor proteins: Polar explorations, *Nature (London)* **376,** 215–216.

Hirose, K., Fan, J., and Amos, L. A. (1995a) Re-examination of the polarity of microtubules and sheets decorated with kinesin motor domain, *J. Mol. Biol.* **251,** 329–333.

Hirose, K., Lockhart, A., Cross, R. A., and Amos, L. A. (1995b) Nucleotide-dependent angular change in kinesin motor domain bound to tubulin, *Nature (London)* **376,** 277–279.

Hirose, K., Lockhart, A., Cross, R. A., and Amos, L. A. (1996) Three-dimensional cryo-electron microscopy of dimeric kinesin and ncd motor domains on microtubules, *Proc. Natl. Acad. Sci. USA* **93,** 9539–9544.

Hoenger, A., Sablin, E. P., Vale, R. D., Fletterick, R. J., and Milligan, R. A. (1995) 3-Dimensional structure of a tubulin-motor protein complex, *Nature (London)* **376,** 271–274.

Hoenger, A., and Milligan, R. A. (1996) Polarity of 2-D and 3-D maps of tubulin sheets and motor-decorated sheets, *J. Mol. Biol.* **263,** 114–119.

Hoenger, A., and Milligan, R. A. (1997) Motor domains of kinesin and ncd interact with microtubule protofilaments with the same binding geometry. *J. Mol. Biol.* **265,** 553–564.

Kellogg, D. R., Moritz, M., and Alberts, B. M. (1994) The centrosome and cellular organization, *Annu. Rev. Biochem.* **63,** 639–674.

Kikkawa, M., Ishikawa, T., Nakata, T., Wakabayashi, T., and Hirokawa, N. (1994) Direct visualization of the microtubule lattice seam both in vitro and in vivo, *J. Cell Biol.* **127,** 1965–1971.

Kikkawa, M., Ishikawa, T., Wakabayashi, T., and Hirokawa, N. (1995) 3-Dimensional structure of the kinesin head-microtubule complex, *Nature (London)* **376,** 274–279.

Lanzavecchia, S., Bellon, P. L., Dallai, R., and Afzelius, B. A. (1994) Three-dimensional reconstructions of accessory tubules observed in the sperm axonemes of two insect species, *J. Struct. Biol.* **113,** 225–237.

Lockhart, A., Crevel, I. M.-T. C., and Cross, R. A. (1995) Kinesin and ncd bind through a single head to microtubules and compete for a shared MT binding site, *J. Mol. Biol.* **249,** 763–771.

Mandelkow, E. M., Rapp, R., and Mandelkow, E. (1986) Microtubule structure studied by quick freezing: cryo-electron microscopy and freeze fracture, *J. Microsc.* **141,** 361–373.

Mandelkow, E., and Mandelkow, E. M. (1995) Microtubules and microtubule-associated proteins, *Curr. Op. Cell Biol.* **7,** 72–81.

Mitchison, T. J. (1993) Localization of an exchangeable GTP binding site at the plus end of microtubules, *Science* **261,** 1044–1047.

Nogales, E., Wolf, S. G., Khan, I. A., Luduena, R. F., and Downing, K. H. (1995) Structure of tubulin at 6.5 Å and location of the taxol-binding site, *Nature (London)* **375,** 424–427.

Song, Y.-H., and Mandelkow, E. (1993) Recombinant kinesin motor domain binds to β-tubulin and decorates microtubules with a B surface lattice, *Proc. Natl. Acad. Sci. USA* **90,** 1671–1675.

Song, Y.-H., and Mandelkow, E. (1995) The anatomy of flagellar microtubules: polarity, seam, junctions, and lattice, *J. Cell Biol.* **128,** 81–94.

Thaler, C. D., and Haimo, L. T. (1996) Microtubules and microtubule motors: Mechanisms of regulation, *Int. Rev. Cytol.* **164,** 269–327.

Trachtenberg, S., and DeRosier, D. J. (1987) Three-dimensional structure of the frozen-hydrated flagellar filament: The left-handed filament of *Salmonella tymphimurium, J. Mol. Biol.* **195,** 581–601.

Turner, D., Chang, C., Fang, K., Cuomo, P., and Murphy, D. (1996) Kinesin movement on glutaraldehyde-fixed microtubules, *Anal. Biochem.* **242,** 20–25.

Vigers, G. P. A., Crowther, R. A., and Pearse, B. M. F. (1986) Three-dimensional structure of clathrin cages in ice, *EMBO J.* **5,** 529–534.

Wade, R. H., and Chrétien, D. (1993) Cryoelectron microscopy of microtubules, *J. Struct. Biol.* **110,** 1–27.

Walker, R. A. (1995) Ncd and kinesin motor domains interact with both alpha-tubulin and beta-tubulin, *Proc. Natl. Acad. Sci. USA* **92,** 5960–5964.

Wolf, S. G., Mosser, G., and Downing, K. H. (1993) Tubulin conformation in zinc-induced sheets and macrotubes, *J. Struct. Biol.* **111,** 190–199.